Ice Shelves and Seasonal Discharge Calculation

Chris MacMackin

June 3, 2016

In order to understand the impact of seasonal variations in subglacial discharge on the structure of an ice shelf, a greatly simplified linearized model was derived. This was done in a similar manner to that of Dallaston et al. (2015), using many of the same assumptions. The derivation of these equations is described below, along with information on how a numerical solution was obtained and the subsequent analysis performed.

1 Theory

1.1 Shelf and Plume Equations

An ice shelf can be modelled in one dimension with the equations

$$\frac{\partial h}{\partial t} + \frac{\partial}{\partial x}(hu) = -(\rho_o/\rho_i)m, \tag{1}$$

$$\frac{\partial}{\partial x}\left(4\eta h\frac{\partial u}{\partial x}\right) - \left(1 - \frac{\rho_i}{\rho_o}\right)\rho_i g h\frac{\partial h}{\partial x} = 0, \tag{2}$$

where η is the effective viscosity of ice, h is the thickness of the ice shelf, u is the x-component of the ice shelf velocity (with the y-component assumed to be zero), ρ_i is the density of ice, ρ_o is the reference density of sea water, g is the gravitational acceleration, and m is the melt rate of the ice shelf. Normally a power law is used to relate η to the strain rate of ice deformation (Glen's law), but for simplicity η is treated as a constant here, which would make ice a Newtonian fluid.

When modelling the melt rate, it is assumed that the ice shelf temperature is already close to the melting temperature, T_m, and that the melting temperature does not depend on salinity. This results in a greatly simplified thermal dynamics compared to those seen in most numerical treatments of ice shelves. The melting is described by

$$mL = c\gamma_T|U|(T - T_m), \tag{3}$$

where L is the latent heat of fusion for the ice, c is the specific heat of ocean water, γ_T is a dimensionless coefficient representing heat transfer, U is the x-component of the velocity of the plume (the ocean boundary layer adjacent to the bottom of the ice shelf), and T is the plume temperature.

In modelling the motion of the plume underneath the ice shelf, it is assumed that thermal expansion is negligible and that salinity is the primary control of density:

$$\rho_a - \rho = \rho_o\beta_S S_\Delta, \qquad S_\Delta = S_a - S. \tag{4}$$

Here, ρ_a is the ambient ocean density, ρ the density of the plume, β_S the haline contraction coefficient, S_Δ the salinity deficit of the plume, S_a the salinity of the ambient ocean (assumed to be constant), and S the salinity of the plume. The plume's behaviour is then described by equations representing conservation of mass, momentum, salinity, and heat:

$$\frac{\partial}{\partial x}(DU) = e + m, \tag{5}$$

$$\frac{\partial}{\partial x}(DU^2) = Dg\beta_S S_\Delta \left(\frac{\partial b}{\partial x} - \frac{\partial D}{\partial x}\right) + \frac{\partial}{\partial x}\left(\kappa D \frac{\partial U}{\partial x}\right) - C_d|\vec{U}|U - \frac{gD^2\beta_S}{2}\frac{\partial S_\Delta}{\partial x}, \quad (6)$$

$$\frac{\partial}{\partial x}(DUS) = eS_a + \frac{\partial}{\partial x}\left(\kappa D \frac{\partial S}{\partial x}\right) + mS_i, \quad (7)$$

$$\frac{\partial}{\partial x}(DUT) = eT_a + \frac{\partial}{\partial x}\left(\kappa D \frac{\partial T}{\partial x}\right) + mT_m - \frac{mL}{c}. \quad (8)$$

D represents the plume thickness, e the entrainment rate, b the basal depth of the ice shelf, κ the turbulent eddy diffusivity in the plume, C_d the turbulent drag coefficient, and $S_i \approx 0$ the salinity of the ice shelf. Assuming hydrostatic balance,

$$b = -(\rho_i/\rho_o)h. \quad (9)$$

The entrainment is parameterized as

$$e = E_0|U|\left|\frac{\partial b}{\partial x}\right|, \quad (10)$$

where E_0 is a dimensionless constant.

The ice shelf is given boundary conditions

$$h(0) = h_g, \quad h(X) = 0, \quad u(0) = u_g, \quad (11)$$

where $x = X$ is the calving front and coordinates are chosen such that $x = 0$ is the grounding line of the ice shelf. There is taken to be a volume flux of subglacial discharge, Q_g, initiating the flow at the grounding line. As it is formed from melting of the glacier, it is at the melting temperature of water and has no salinity. The speed of its outflow is prescribed.

$$D(0)U(0) = Q_g, \qquad U(0) = U_g, \qquad S(0) = 0, \qquad T(0) = T_m, \quad (12)$$

No boundary conditions are specified at the calving front, meaning that the plume is implicitly assumed to be supercritical.

1.2 Non-dimensionalization

Prior to simplifying and dropping small terms, the equations in §1.1 were converted to a dimensionless form. In order to do this, various dimensionless parameters were introduced. Equations (1) and (2) suggest the parameters

$$r \equiv \frac{\rho_o}{\rho_i} \qquad \gamma \equiv \frac{(1-\rho_i/\rho_o)\rho_i g h_0 x_o}{4\eta u_o}, \qquad \lambda \equiv \frac{\rho_o m_0 x_0}{\rho_i h_0 u_0}, \quad (13)$$

to describe the ice shelf, where a variable followed by a subscript nought is the representative value by which the dimensional form of that variable must be divided to obtain its dimensionless form. Here, r is the density ratio, γ represents the ratio of hydrostatic to viscous forces in the ice (quantifying the amount of stretching to occur), while λ represents the ratio of the melt rate to the mass flux of ice through the grounding line.

In order to non-dimensionalize equations (3)–(10), the following six parameters were adopted to describe the plume:

$$\begin{gathered} \epsilon_m \equiv \frac{m_0 x_0}{D_0 U_0}, \qquad \epsilon_g \equiv \frac{Q_{g0}}{D_0 U_0}, \qquad \nu \equiv \frac{\kappa}{U_0 x_0}, \\ \mu \equiv \frac{C_d x_0}{D_0}, \qquad \delta \equiv \frac{D_0}{h_0} = E_0, \qquad \beta \equiv \frac{c(T_a - T_m)}{L}. \end{gathered} \quad (14)$$

Table 1: Typical values for the parameters used in the nondimensional form of the couple plume/ice shelf equations. These are the same values as used by Dallaston et al. (2015), with the exception of γ, which has a slightly different definition here.

Parameter	Description	Typical Value
r	density ratio	1.12
γ	dimensionless stretching rate	2
λ	dimensionless melt rate	0.37
ν	dimensionless eddy diffusivity	0.0022–0.022
δ	dimensionless buoyancy correction	0.036
ϵ_g	subglacial flux/entrained flux	1.1×10^{-3}
ϵ_m	subglacial melt/entrained flux	6.9×10^{-4}
μ	dimensionless drag coefficient	1.27
β	inverse Stefan number	0.024

These represent the ratios of subglacial melt to entrained flux, subglacial volume flux to entrained flux, eddy diffusivity to inertia, drag coefficient to aspect ratio of the domain, characteristic thickness of the plume to the ice shelf (a buoyancy correction), and inverse Stefan number. Typical values for these parameters can be found in table 1.

We use

$$\begin{aligned} U_0 &= \left(\frac{Q_{g0} g \beta_S S_a}{E_0}\right)^{1/3}, \qquad m_0 = \frac{c\gamma_T U_0 (T_a - T_m)}{L}, \\ D_0 &= E_0 h_0, \qquad S_{\Delta 0} = \frac{Q_{g0} S_a}{D_0 U_0}, \qquad T_{\Delta 0} = \frac{\gamma_T x_0}{D_0}(T_a - T_m), \end{aligned} \tag{15}$$

for the plume variables, with the temperature deficit $T_\Delta \equiv T_a - T$. The characteristic timescale of advection was $T_0 = x_0/u_o$.

1.3 Simplified Equations

Using the above parameters, the equations for the ice shelf can be written in a non-dimensional form:

$$\frac{\partial h}{\partial t} + \frac{\partial}{\partial x}(hu) = -\lambda m. \tag{16}$$

$$\frac{\partial}{\partial x}\left(h\frac{\partial u}{\partial x}\right) - \gamma h \frac{\partial h}{\partial x} = 0, \tag{17}$$

The nondimensional form of the melt rate is

$$m = |U|\left(1 - \frac{\epsilon_m}{\beta} T_\Delta\right) \tag{18}$$

and $b = r^{-1}h$. The plume equations have the dimensionless form

$$\frac{\partial}{\partial x}(DU) = |U|\left|\frac{\partial b}{\partial x}\right| + \epsilon_m m, \tag{19}$$

$$\frac{\partial}{\partial x}(DU^2) = DS_\Delta\left(\frac{\partial b}{\partial x} - \delta\frac{\partial D}{\partial x}\right) + \nu\frac{\partial}{\partial x}\left(D\frac{\partial U}{\partial x}\right) - \mu|U|U - \frac{\delta D^2}{2}\frac{\partial S_\Delta}{\partial x}, \tag{20}$$

$$\frac{\partial}{\partial x}(DUS_\Delta) = \frac{\epsilon_m}{\epsilon_g} m + \nu\frac{\partial}{\partial x}\left(D\frac{\partial S_\Delta}{\partial x}\right), \tag{21}$$

$$\frac{\partial}{\partial x}(DUT_\Delta) = \beta m + m + \nu\frac{\partial}{\partial x}\left(D\frac{\partial T_\Delta}{\partial x}\right). \tag{22}$$

Note that the following boundary conditions at the grounding line look somewhat different in their dimensionless form than the form in equation (12):

$$DU = \epsilon_g Q_g, \qquad U = U_g. \qquad S_\Delta = \frac{1}{\epsilon_g}, \qquad T_\Delta = \frac{\beta}{\epsilon_m}. \tag{23}$$

In order to make the plume equations tractable for an analytic solution, various terms need to be dropped. It is assumed that the heat entering the plume due to entrainment is much greater than that lost to melting the ice shelf. Then

$$\text{melting rate} \times \text{latent heat} \ll \text{ocean heat} \times \text{entrainment}$$

$$\Rightarrow \frac{\text{melting rate}}{\text{entrainment}} \ll \frac{\text{ocean heat}}{\text{latent heat}}$$

$$\therefore \epsilon_m \ll \beta.$$

The turbulent drag will be treated as negligible ($\mu \ll 1$).[1] Entrainment is assumed to be the dominant source of specific mass flux for the plume, dominating over both melting and subglacial discharge. However, subglacial discharge is taken to be the dominant source of buoyancy, compared to melting. As such

$$\epsilon_m \ll \epsilon_g \ll 1.$$

The scale for the thickness of the plume is much smaller than that for the ice shelf ($\delta \ll 1$) and the plume's thickness is assumed not to change rapidly. Finally, eddy diffusivity is neglected ($\nu \ll 1$).

Using these assumptions and defining the buoyancy $B \equiv DS_\Delta$ allows equations (18)–(22) to be simplified to

$$m = |U|, \tag{24}$$

$$\frac{\partial}{\partial x}(DU) = |U| \left| \frac{\partial b}{\partial x} \right|, \tag{25}$$

$$\frac{\partial}{\partial x}(DU^2) = B\frac{\partial b}{\partial x}, \tag{26}$$

$$\frac{\partial}{\partial x}(BU) = 0, \tag{27}$$

$$\frac{\partial}{\partial x}(DUT_\Delta) = (\beta + 1)m. \tag{28}$$

It has been implicitly assumed that U is everywhere non-negative and that b is monotonically increasing, so that the absolute values are no longer required. Note that temperature has now become uncoupled from this system, meaning equation (28) can henceforth be ignored.

1.4 Steady-State Solution

Using the transformation

$$\frac{\partial}{\partial x} = \frac{\partial b}{\partial x}\frac{\partial}{\partial z},$$

the plume equations can be converted to

$$\frac{\partial}{\partial z}(DU) = U, \qquad \frac{\partial}{\partial z}(DU^2) = B, \qquad \frac{\partial}{\partial z}(BU) = 0 \tag{29}$$

[1] This is the most problematic of the assumptions made; it is demonstrably false on the scale typically associated with ice shelves. As such, the solutions to the resulting equations will only be quantitatively accurate near the grounding line, where the μ can be shown to be small when $x_0 \sim 1\,\text{km}$.

The latter-most of these can easily be seen to yield

$$B = \frac{Q_g}{U}. \tag{30}$$

Using the substitution $Q = DU$, defining $M \equiv QU$, and integrating the second equation in (30) with respect to Q yields the solution

$$U = \frac{Q_g^{1/3}(\epsilon_g^3 U_g^3 Q_g^2 - \epsilon^3 Q_g^3 + Q^3)^{1/3}}{Q}, \qquad z - b(0) = \int_{\epsilon_g}^{Q/Q_g} \frac{Q_g^{2/3} q}{\left(\epsilon_g^3 U_g^3/Q_g - \epsilon_g^3 + q^3\right)^{1/3}} dq. \tag{31}$$

In the case $\epsilon_g \to 0$ this reduces to

$$D = z - b(0) = (h_g - h(x))/r, \qquad U = Q_g^{1/3}, \qquad B = Q_g^{2/3}, \tag{32}$$

which will not necessarily satisfy the boundary conditions at the grounding line. However, it can be shown that, for small but nonzero values of ϵ_g, the solution in equation (31) converges to equation (32) outside of a small boundary layer in which the boundary conditions are satisfied (Dallaston et al., 2015). As such, the limit $\epsilon_g \to 0$ will be taken and the simpler set of equations used, with the new boundary conditions

$$D(0) = 0, \qquad U(0) = Q_g^{1/3}, \qquad B(0) = Q_g^{2/3}. \tag{33}$$

As Q_g is scaled by Q_{g0}, the value of which can be set arbitrarily, it can be set to be 1. Using the solution for the plume, the ice shelf has the following steady-state equations:

$$\frac{\partial}{\partial x}(hu) = -\lambda, \qquad \frac{\partial}{\partial x}\left(h\frac{\partial u}{\partial x}\right) - \gamma h \frac{\partial h}{\partial x} = 0. \tag{34}$$

Choosing boundary conditions $h_g = u_g = 1$ for the inflowing ice and $h \to 0$ as $x \to X$ for the end of the ice shelf, these equations can be integrated to show

$$X = \frac{1}{\lambda}, \qquad u = \sqrt{1 + \frac{\gamma}{2}X - \frac{\gamma}{2}X(1 - x/X)^2}, \qquad h = \sqrt{\frac{(1 - x/X)^2}{1 + \frac{\gamma}{2}X - \frac{\gamma}{2}X(1 - x/X)^2}}. \tag{35}$$

1.5 Linearization

In order to investigate how the ice shelf responds to seasonal variations in subglacial discharge, a linear perturbation analysis was performed. The different variables in equations (16), (17), and (25)–(27) were taken to have solutions oscillating about the steady state with the form:

$$h(x,t) = \bar{h}(x) + \tilde{h}(x)e^{i\omega t}, \tag{36}$$

where $\bar{h}$ is the steady state solution, $\tilde{h}$ represents the variations in x of the time-dependent component of the solution, and ω is the angular frequency of oscillations. Substituting into the aforementioned five equations and keeping only terms of first order in the perturbed variables, the linearized equations were found to be

$$(\tilde{h}\bar{u} + \bar{h}\tilde{u})' + i\omega\tilde{h} = -\lambda\tilde{U}, \tag{37}$$

$$(\tilde{h}\bar{u}' + \bar{h}\tilde{u}')' - \gamma(\bar{h}\tilde{h})' = 0, \tag{38}$$

$$\bar{D}\tilde{U}' + \tilde{D}'\bar{U} = -\frac{\bar{U}}{r}\frac{\partial\tilde{h}}{\partial x}, \tag{39}$$

$$\bar{D}\bar{U}\tilde{U}' + 2\bar{U}\tilde{U}\bar{D}' = -\frac{\tilde{B}}{r}\frac{\partial\bar{h}}{\partial x}, \tag{40}$$

$$\bar{B}\tilde{U}' + \tilde{B}'\bar{U} = 0. \tag{41}$$

Note that these results make use of the relationship $b = -h/r$ and the fact that $\bar{U}^2 = \bar{B}$ and $\bar{U}' = \bar{B}' = 0$. When deriving equation (40), two terms containing the gradient in $\tilde{h}$ cancel. Physically, this occurs because any increase in the buoyancy force that results from a steeper slope is exactly compensated by additional entrainment of (denser) ambient water into the plume as a result of the increased slope. This cancellation would not necessarily happen if a different parameterisation of entrainment were used.

The subglacial discharge is prescribed to vary according to

$$Q_g = 1 + \tilde{Q}_g e^{i\omega t}. \tag{42}$$

Recalling the results for U and B in equation 32 and applying the binomial approximation, the linearised boundary conditions for $\tilde{U}$ and $\tilde{B}$ were determined, with all other perturbations assumed to be zero at the grounding line:

$$\tilde{U}(0) = \tfrac{1}{3}\tilde{Q}_g, \quad \tilde{B}(0) = \tfrac{2}{3}\tilde{Q}_g, \quad \tilde{D}(0) = 0, \quad \tilde{h}(0) = 0, \quad \tilde{u}(0) = 0. \tag{43}$$

The position of the end of the ice shelf is taken to vary according to

$$X = \bar{X} + \tilde{X}e^{i\omega t}, \tag{44}$$

where $\bar{h}(\bar{X}) = 0$. Performing a Taylor expansion of $h(X)$ about $\bar{X}$, it can be shown that

$$\tilde{X} \approx -\frac{\tilde{h}(\bar{X})}{\bar{h}'(\bar{X})}. \tag{45}$$

The degeneracy in equation (38) due to $\bar{h} \to 0$ at $x = \bar{X}$ means that it is not necessary to specify a boundary condition here; it is only necessary to ensure that the solution remains bounded and satisfies equation (38) at $x = X$. Using the relationship $2\bar{u}' = \gamma\bar{h}$ and $\bar{h}(X) = baru'(X) = 0$, this can be shown to be equivalent to requiring

$$\tilde{u}'(\bar{X}) = \tfrac{1}{2}\gamma\tilde{h}(\bar{X}). \tag{46}$$

Note that $\tilde{D}$ is only present in equation (39), meaning that it is uncoupled from the rest of the system. As such, $\tilde{D}$ is not solved for directly, but can be diagnosed from other variables.

2 Numerical Solution

2.1 Algorithm

Letting $\boldsymbol{u}$ be the solution vector, a linear system $A\boldsymbol{u} = \boldsymbol{b}$ was constructed and solved. $\boldsymbol{u}$ consisted of the values of the variables h, u, U, and B at Chebyshev collocation nodes across the domain $x \in (0, X]$: $\boldsymbol{u} = (\tilde{h}(x_1), \tilde{h}(x_2), \ldots, \tilde{h}(x_N), \tilde{u}(x_1), \tilde{u}(x_2), \ldots, \tilde{u}(x_N), \tilde{U}(x_1), \tilde{U}(x_2), \ldots, \tilde{U}(x_N), \tilde{B}(x_1), \tilde{B}(x_2), \ldots, \tilde{B}(x_N))$, where N was the number of Chebyshev collocation nodes used. Points at $x = 0$ were not included as these were prescribed from the boundary conditions. In order for the Chebyshev psuedo-spectral method to work correctly, it must be applied to functions which have homogeneous boundary conditions. This was achieved by redefining $\tilde{h}$ to be the deviation from the boundary condition $\tilde{h_0}$, with the same approach applied to the other variables. Any occurrence of $\tilde{h}$ in the system was replaced with $\tilde{h} + \tilde{h}_0$ and all terms containing $\tilde{h}_0$ were placed on the right hand side of the equations ($\boldsymbol{b}$). Derivatives were represented in A using the Chebyshev differentiation matrix (D_x) appropriate for the number of nodes selected. Using the relation $\gamma\bar{h} = 2\bar{u}'$, it can thus be seen that

$$A = \begin{bmatrix} i\omega I + \bar{\boldsymbol{u}}'^T I + \bar{\boldsymbol{u}}^T D_x & \bar{\boldsymbol{h}}'^T I + \bar{\boldsymbol{h}}^T D_x & \lambda I & 0 \\ -\bar{\boldsymbol{u}}''^T I + \bar{\boldsymbol{u}}'^T D_x & \bar{\boldsymbol{h}}'^T D_x + \bar{\boldsymbol{h}}^T D_x^2 & 0 & 0 \\ 0 & 0 & -2\bar{\boldsymbol{h}}'^T(\bar{\boldsymbol{U}}^T I) + (\bar{\boldsymbol{h}}_{\boldsymbol{g}} - \bar{\boldsymbol{h}})^T(\bar{\boldsymbol{U}} D_x) & \bar{\boldsymbol{h}}'^T I \\ 0 & 0 & \bar{\boldsymbol{B}}^T D_x & \bar{\boldsymbol{U}}^T D_x \end{bmatrix} \tag{47}$$

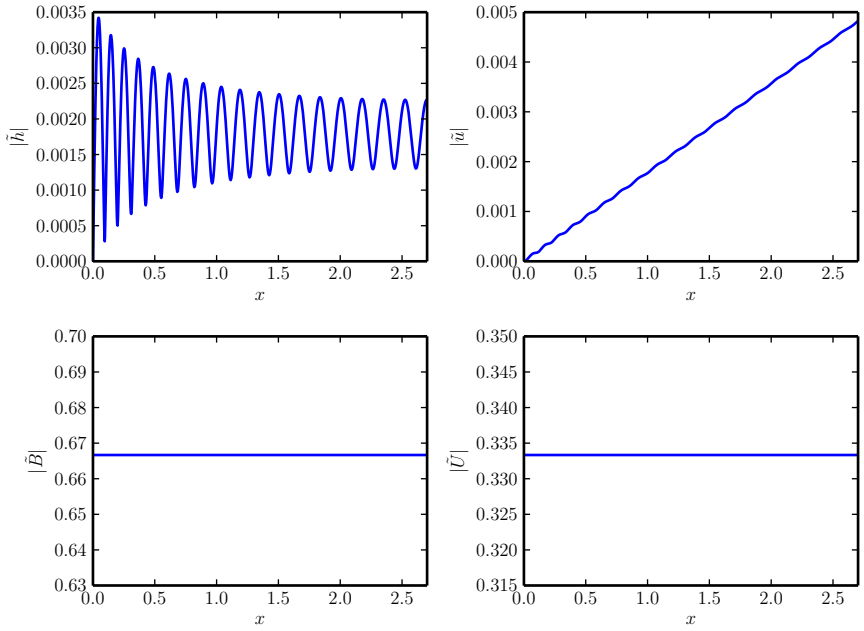

Figure 1: The magnitudes of the linear perturbations to the ice shelf. Oscillatory behaviour is clear in $\tilde{h}$ and its effects can be seen in the ripples in $\tilde{u}$. Note, however, that the perturbations to the plume, $\tilde{U}$ and $\tilde{B}$, do not change from the boundary conditions across the entire domain. Be aware that it is the real components of the perturbed variables which corresponds to the actual perturbations at a given time, rather than the magnitude.

$$\boldsymbol{b} = \begin{bmatrix} -\tilde{h}(x_0)(i\omega + \bar{\boldsymbol{u}}') - \tilde{u}_0\bar{h}' - \lambda\tilde{U}(x_0) \\ \tilde{h}(x_0)\bar{\boldsymbol{u}}'' \\ (2\tilde{U}(x_0) - \tilde{B}(x_0))\bar{\boldsymbol{h}}' \\ \mathbf{0} \end{bmatrix}. \tag{48}$$

This system was solved using the `scipy` package in Python. The solutions were tested for convergence, which was found to occur when about 90 Chebyshev nodes were used and provided about 8 digits of accuracy. This may have been an overly pessimistic result, as interpolation was required in order to compare solutions to the "exact" (high resolution) one, which introduced additional error. It was found that 200 nodes were adequate for numerical purposes, but small scale variations were not resolved sufficiently for display unless 800 nodes were used.

2.2 Results

The equations (37)–(41) make up a linear system with amplitude controlled by the initiating flux Q_g. The spatial structure of perturbations was found by solving with $Q_g = 1$. Note that the amplitudes of perturbations for other values of Q_g can be determined by rescaling.

The solution to this system consists of complex numbers. As such, both its magnitude (figure 1) and its phase (figure 2) must be plotted. In the latter it can be seen that the phase of $\tilde{h}$ oscillates around $\pi/2$, while that of $\tilde{u}$ asymptotically approaches this value. The reason that these variables are out of phase with Q_g is because changes to thickness caused by increased melting associated with high subglacial discharge require a quarter of a cycle to accumulate and reach a maximum. As it is changes to thickness which cause changes in velocity, the speed of the ice would also be out of phase.

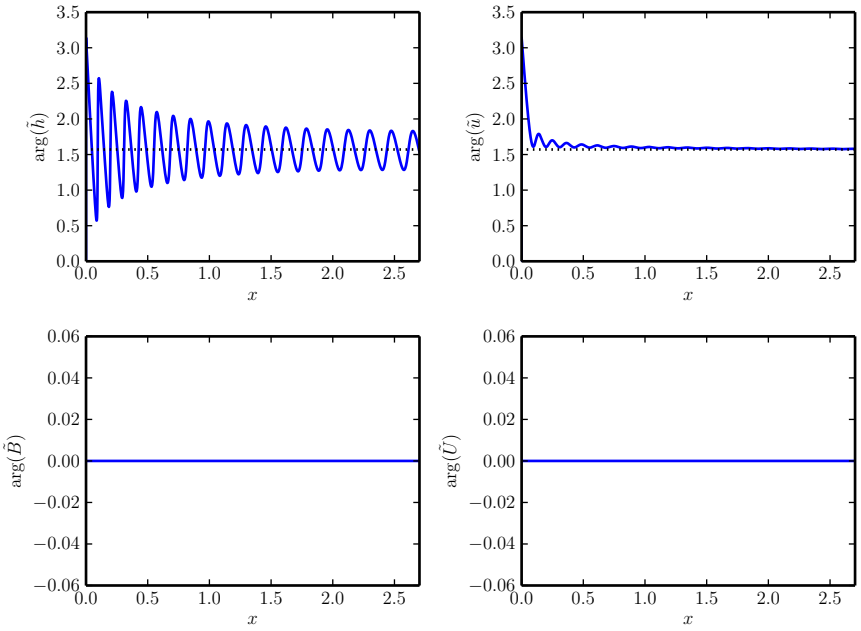

Figure 2: The phases of the linear perturbations to the ice shelf. Variations can be seen in the phases of the ice shelf variables, $\tilde{h}$ and $\tilde{u}$. The phase of $\tilde{h}$ oscillates about $\pi/2$ (black dotted line), while that of $\tilde{u}$ asymptotically approaches it. However, the phases of the plume variables, $\tilde{B}$ and $\tilde{U}$, remain constant at zero.

The solution is more easily understood by plotting the real component of $\tilde{h}e^{i\omega t}$ at various times during the seasonal cycle (see figure 3). This reveals two different responses to the seasonal forcing. One is the formation of ripples in the ice shelf, which propagate towards the calving front over time. The other is a global oscillation in the thickness of the ice shelf over the course of a year. It may at first seem that the latter effect would require some refreezing to occur, which is in violation of the model used here. However, closer analysis reveals that the switch of $\tilde{h}$ from negative to positive is a result of individual ice parcels melting more slowly as they are advected than they were in the base state. This can be demonstrated by computing the Lagrangian derivative of the perturbation, $D_t(\tilde{h}e^{i\omega t}) = \partial_t(\tilde{h}e^{i\omega t}) + \bar{u}\partial_x\tilde{h}e^{i\omega t} = i\omega\tilde{h}e^{i\omega t} + \bar{u}\tilde{h}'e^{i\omega t}$, which is revealed to be smaller than the Lagrangian derivative of the background, $D_t\bar{h} = \bar{u}\partial_x\bar{h}$, at all times.

2.3 Analysis

In order to better understand the result, the magnitudes of individual components of the system—i.e. equation (37)–(41) or (47) and (48)—were plotted (see figure 4). The first plot (ice continuity) is the most important part of this figure; it demonstrates that the $i\omega\tilde{h}$, $\bar{u}\tilde{h}'$, and $-\lambda\tilde{U}$ terms in the continuity equation for ice are much larger than any of the remaining terms (which represent stretching processes). Using the expression for $\frac{D}{Dt}\tilde{h}e^{i\omega t}$ derived earlier, it can be seen that the leading order balance in the conservation of ice mass in equation (37) is

$$\frac{D}{Dt}\tilde{h}e^{i\omega t} \approx -\lambda\tilde{U}e^{i\omega t}. \tag{49}$$

This result has important implications and allows for an understanding of the behaviour of the ice shelf as a whole. At any given time, all ice across the shelf will be experiencing the same rate of change in perturbed thickness. The global oscillations in the shelf's thickness

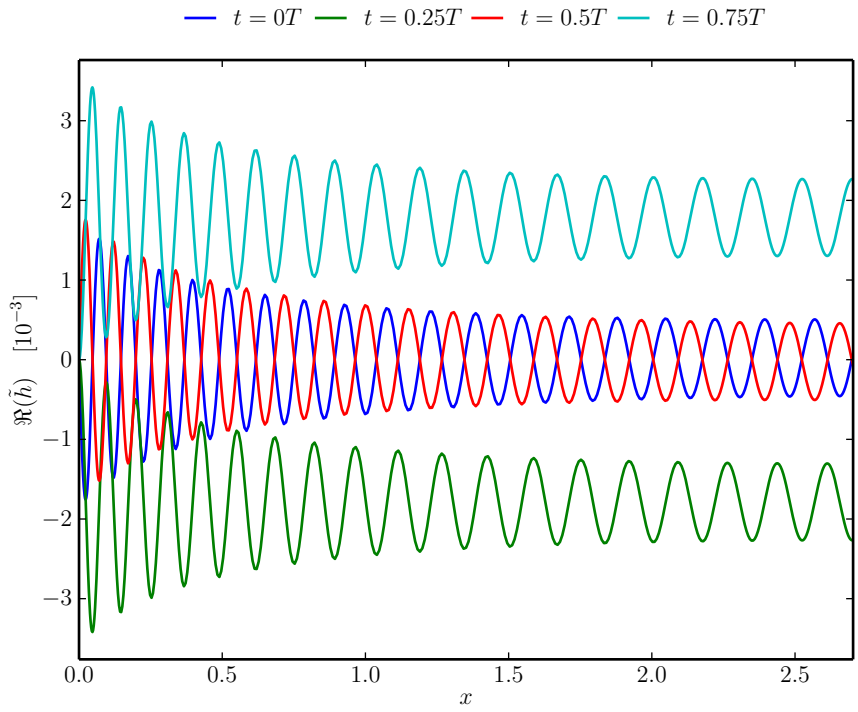

Figure 3: The real component of the perturbation to the ice thickness, $\tilde{h}e^{i\omega t}$, at various times during the oscillatory period ($T = 2\pi/\omega$). Two effects can be observed here: the development of ripples which propagate along the ice shelf, and overall oscillations in ice shelf thickness.

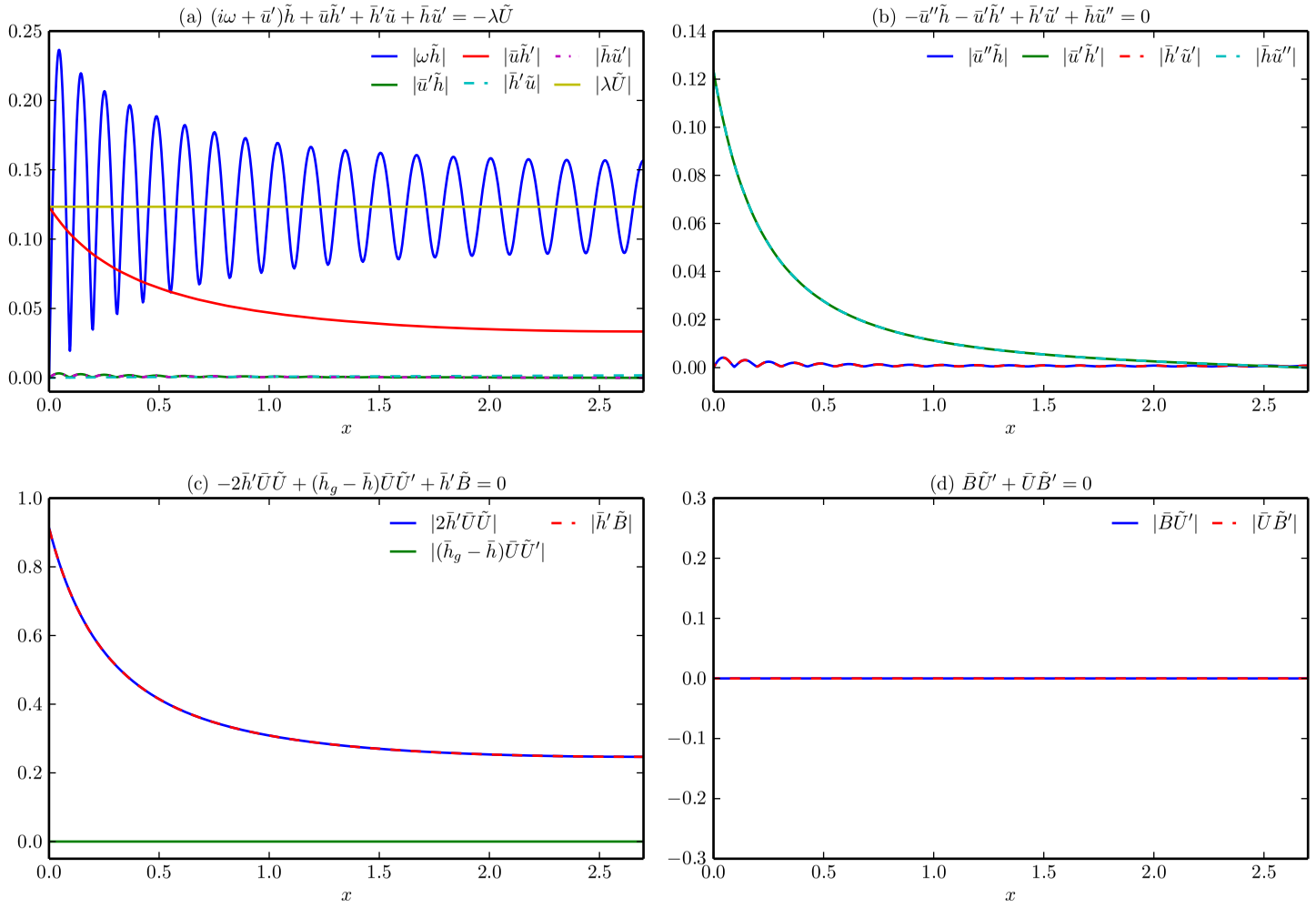

Figure 4: The magnitudes of individual components of the linearized equations. Each subplot represents a different equation: (a) continuity of ice, (b) conservation of ice momentum, (c) conservation of plume momentum, (d) conservation of salt.

are the logical consequence of this uniform melting. To see why the ripples form, consider a time $t_g(x)$ which represents the time the parcel of ice located at x crossed the grounding line. From the boundary condition, $\tilde{h}$ is 0 for the ice parcel at that time. Integrating equation (49) reveals that the thickness of this ice parcel at a given time is then

$$\tilde{h}(t) = \frac{i\lambda\tilde{U}}{\omega}\left(1 - e^{i\omega(t-t_g)}\right). \tag{50}$$

Clearly, the perturbation to the ice shelf thickness oscillates with t_g. Given that $\bar{u}$ is monotonic increasing with x and $\tilde{u}$ is small, t_g is also monotonic increasing with x. As such, the perturbed ice thickness also oscillates with x, explaining the ripples and the fact that ripples are not a perfect sinusoid. Putting all of this in physical terms, ice which crosses the grounding line when the discharge (and hence melting) is high will experience more melting by the time it reaches the end of the ice shelf than would ice which crosses the grounding line when the discharge is low, causing these two parcels of ice to have different thicknesses.

By tracking the the position of individual peaks and troughs of the ripples over time, the phase speed of the ripples can be determined. The speed of a given peak/trough was found to be in near perfect agreement with the local velocity of the ice.

The second plot in figure 4 (ice momentum) shows that $\gamma\tilde{h} \approx 2\tilde{u}'$, as was exactly the case for the steady state variables. This indicates that, as in the steady state, stretching is driven by changing hydrostatic pressure. The third plot (plume momentum) reveals $-2\bar{h}'\bar{U}\tilde{U} + \bar{h}'\tilde{B} = 0$, meaning that momentum fluxes within the plume are driven by the buoyancy. The balance in the final plot (salt) is trivially satisfied as both $\tilde{U}$ and $\tilde{B}$ are constant due to the choice of entrainment parameterisation removing any dependence between them and the slope of the ice shelf base.

2.4 Varying Parameters

By varying the driving frequency, ω, a dispersion relationship was obtained. Initial attempts to determine a wave-number using a Fourier transform proved troublesome because the spectrum lacked a clean peak. The most effective way to estimate a representative wavelength ultimately proved to be measuring the distance between the first peak and trough in $\Re(\tilde{h})$. The average value of $\bar{u}$ was also found over this range. These results are plotted below in figure 5, revealing the relationship

$$\omega \approx k\bar{u} \tag{51}$$

where $\bar{u}$ is the average of the local velocities at the peak and trough. This is what would be expected given that the "waves" are transported via advection of the ice. It is the changing value of $\bar{u}$ along the ice shelf which causes changes to the ripples' wavelengths. Note that the aforementioned technique revealed identical results when applied to the last peak and trough on the ice shelf. Smaller values of frequency ω result in ripples with larger amplitudes, as there is more time for excess melting to accumulate over each period (see figure 6).

When the amount of viscous stretching, γ, is increased, it leads to a more significant decrease in the amplitude and wave-number of ripples towards the end of the shelf. The opposite is observed when γ is decreased and when $\gamma = 0$ the amplitude and wave-number of the ripples stays constant across the entire shelf. These behaviours are illustrated in figure 7.

Changing the dimensionless melt rate, λ, changes the length of the ice shelf, with the shelf shortening as λ increases, as was already known from equation (35) of the steady state solution. It was found that there was somewhat more stretching in the low-melt cases, as there was more shelf on which this to occur. Stronger melting also increased the amplitude of the ripples, as it increased the effectiveness of the perturbations in the flow of the plume due to subglacial discharge (see figure 8).

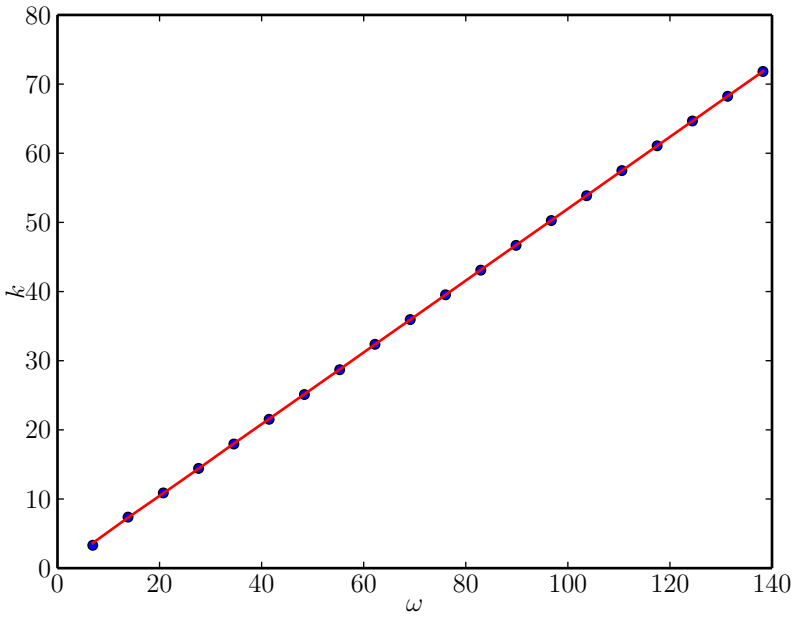

Figure 5: A plot comparing the wave-number of the first ripple in the ice shelf with the driving frequency (circles). Also plotted is the relationship $k\bar{u}$ (line).

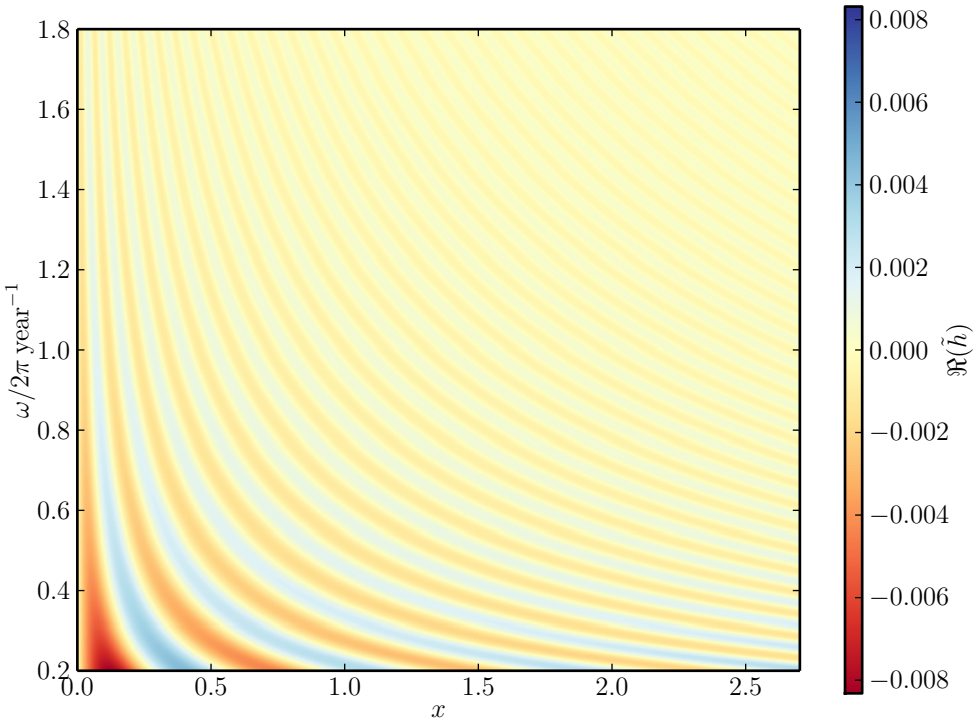

Figure 6: A contour plot of the real component of $\tilde{h}$ along the ice shelf, for different driving frequencies, ω, of the perturbations.

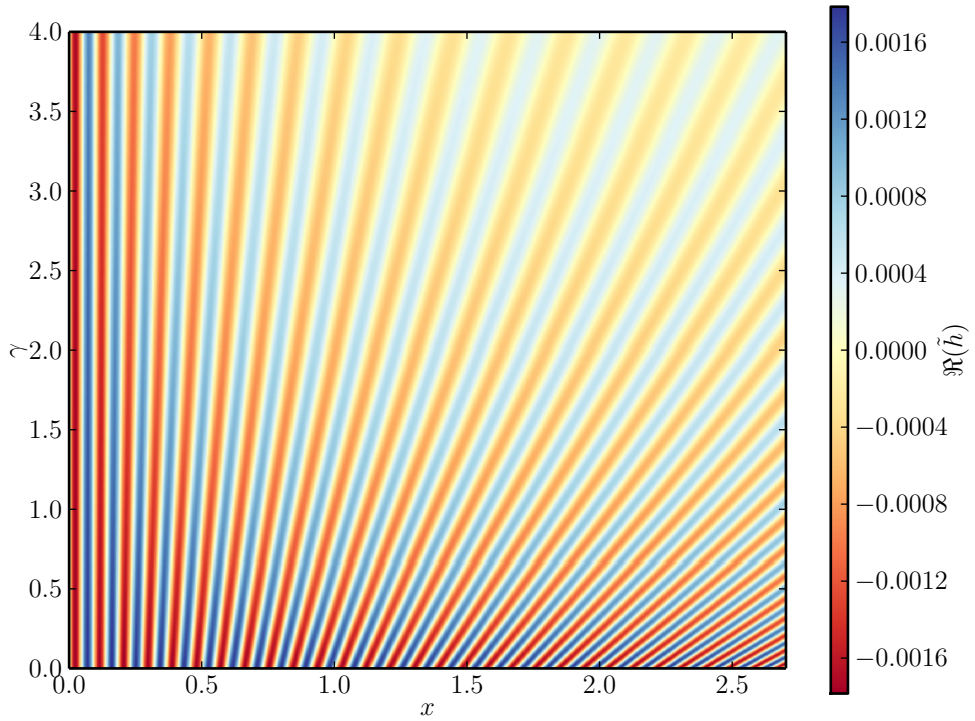

Figure 7: A contour plot of the real component of $\tilde{h}$ along the ice shelf, for various values of the parameter γ, which quantifies stretching of the ice.

By integrating equation (49) from $t = -T/4$ to $t = 0$ (the former being the time at which the ice parcel located at the first peak or trough at $t = 0$ crossed the grounding line) and recalling that $\tilde{U}(x) = \tilde{U}(0)$, it was found that

$$\tilde{h}_{\max} \approx \frac{\lambda \tilde{U}}{\omega}(i-1) \tag{52}$$

However, this proved to be a slight overestimate when the default value of γ, unity, was used (see figure 9a). This is due to the fact that, with the presence of viscous stretching, equation (49) is only an approximate relationship. Stretching causes the amplitude of the ripples to be lower than it would otherwise be due to the combination of advection and melt. However, in the case $\gamma = 0$, no stretching occurs and examining equation (37) reveals that equation (49) becomes exact. In this case, the numerical results match equation (52) exactly (figure 9b).

3 Conclusions

Time-periodic oscillations in subglacial discharge have been seen, in this idealized linear model, to cause two distinct forms of behaviour in ice shelves. On the one hand, they cause the formation of ripples in the ice, which are then advected towards the calving front. On the other, they cause global oscillations in the thickness of the ice shelf over the course of a year. However, the magnitude of both of these modes of behaviour is very small, at only 10^{-3} of the size of the perturbations to the subglacial discharge. Physically this means that, assuming the subglacial discharge actually turned off when it was at its minimum (implying oscillations which would break the small perturbations assumed during

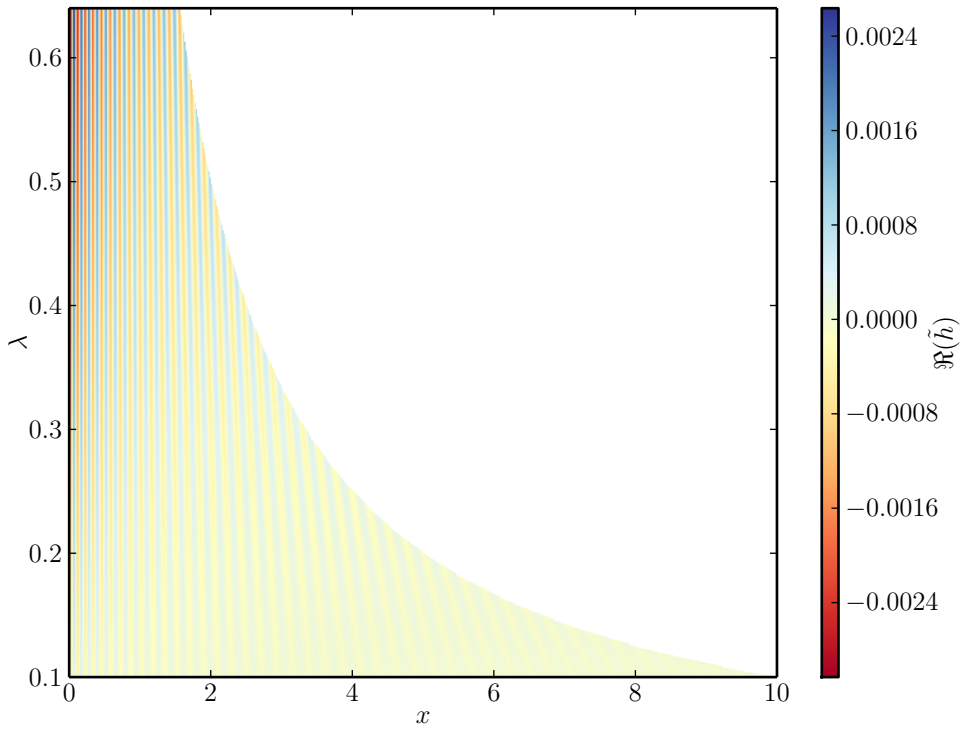

Figure 8: A contour plot of the real component of $\tilde{h}$ along the ice shelf, for various values of the parameter λ, which quantifies melting. Note that the length of the ice shelf is inversely proportional to λ, as seen in equation (35).

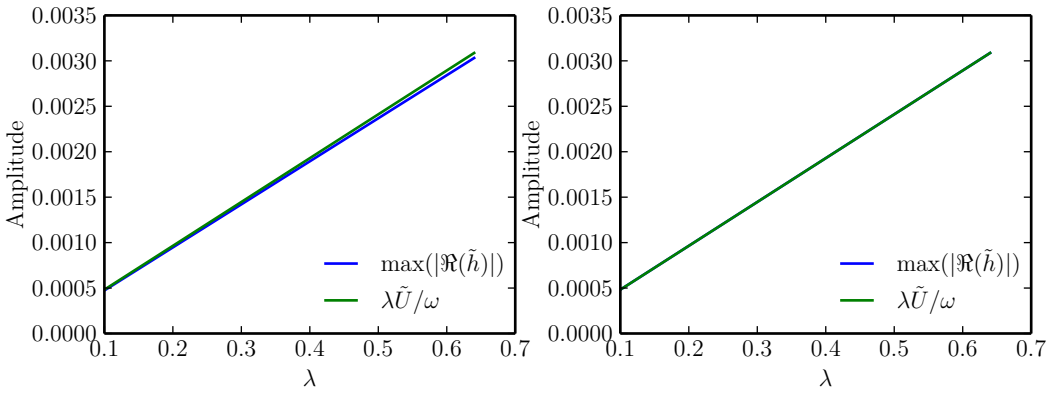

(a) $\gamma = 2$ (b) $\gamma = 0$

Figure 9: The relationship between the maximum absolute value of the real component of $\tilde{h}$ and λ (blue). Also plotted is the relationship expected from equation (52) (green). In the case $\gamma = 0$, these agree perfectly, meaning only the latter is actually visible.

linearisation), changes to the basal topography would be of order 1 m in amplitude. This is two orders of magnitude smaller than channels actually observed.

Both the amplitude and the wave-number of the ripples in the ice increase as the frequency of the oscillations decreases. Increased stretching causes the amplitude of the ripples to decay more quickly along the shelf and for the wave-numbers of ripples near the calving front to become smaller. Increased melting, in addition to shortening the ice shelf, causes the ripples to have larger amplitudes. The perturbation to the ice loss is uniform across the entire shelf and does not vary with the shelf's basal slope as a consequence of the simple slope-dependent parameterisation used for entrainment.

The small scale of the perturbations caused by variations in subglacial discharge likely rule these out as a mechanism variations in ice shelf thickness in the along-flow direction, as observed underneath the Pine Island ice shelf (Bindschadler et al., 2011). Note, however, that this analysis was purely 1 dimensional and as such could not account for any channelization of plume water along the ripples. This could potentially provide a feedback mechanism that increases their melting and may deserve investigation. There could also be some nonlinear effects which this analysis missed. For that reason, the next stage in this research will be to perform a fully non-linear simulation. Eventually the seasonal variations in other values, such as ambient ocean temperature, will be examined as well.

References

R. Bindschadler, D.G. Vaughan, and P. Vornberger. Variability of basal melt beneath the Pine Island Glacier ice shelf, West Antarctica. *Journal of Glaciology*, 57(204):581–595, 2011. ISSN 00221430. doi: 10.3189/002214311797409802. URL http://www.scopus.com/inward/record.url?eid=2-s2.0-80053111927&partnerID=40&md5=6f00dcbf598f638b8644fe7a4995facf.

M.C. Dallaston, I.J. Hewitt, and A.J. Wells. Channelization of plumes beneath ice shelves. *Journal of Fluid Mechanics*, 785:109–134, 2015. ISSN 00221120. doi: 10.1017/jfm.2015.609. URL https://www.scopus.com/inward/record.uri?eid=2-s2.0-84949453149&partnerID=40&md5=9367b6695cc9143a9cffbb31b1f80d05.